Mineralogical Magazine (2022), **86**, 363–372
doi:10.1180/mgm.2022.15

CAMBRIDGE UNIVERSITY PRESS

Article

Ferroberaunite, $Fe^{2+}Fe^{3+}_5(PO_4)_4(OH)_5{\cdot}6H_2O$, a mixed-valence iron member of the beraunite series, from the Gravel Hill mine, Perranzabuloe, Cornwall, England

Jaromír Tvrdý[1]*, Jakub Plášil[2], Luboš Vrtiška[1,3], Jiří Sejkora[3], Radek Škoda[1], Zdeněk Dolníček[3], Martin Petr[4] and František Veselovský[5]

[1]Department of Geological Sciences, Masaryk University, Kotlářská 2, CZ-61137 Brno, Czech Republic; [2]Institute of Physics ASCR, v.v.i., Na Slovance 2, CZ-18221 Praha 8, Czech Republic; [3]Department of Mineralogy and Petrology, National Museum, Cirkusová 1740, CZ-19300 Praha 9, Czech Republic; [4]Regional Centre of Advanced Technologies and Materials, Czech Advanced Technology and Research Institute, Palacký University, Šlechtitelů 27, CZ-78371 Olomouc, Czech Republic; and [5]Czech Geological Survey, Klárov 131/3, CZ-118 21 Praha 1, Czech Republic.

Abstract

The new mineral ferroberaunite, $Fe^{2+}Fe^{3+}_5(PO_4)_4(OH)_5{\cdot}6H_2O$ (IMA2021-36; symbol: *Fbru*), occurs in cavities of 'limonite' iron ore from the Gravel Hill mine, Perranzabuloe, Cornwall, England. Its flattened prismatic crystals up to 400 μm long are dark green to olive green, transparent to translucent, with a vitreous lustre, pearly on cleavages. The Mohs hardness is ~3–4. The density measured by the flotation method is 2.94(2) g·cm^{-3}, the calculated density is 2.907 g·cm^{-3}. Ferroberaunite is biaxial (–), with $\alpha = 1.736(2)$, $\beta = 1.765(3)$, $\gamma = 1.786(5)$ at 589 nm, $2V_{meas.} = 68(3)°$, $2V_{calc.} = 79°$; dispersion of optical axes is strong, $r > v$; orientation is $Y = \mathbf{b}$; $X \approx \mathbf{a}$, $Z \approx \mathbf{c}$. Pleochroism is strong: X = bluish-green >> Z = green > Y = yellow. Electron-microprobe analyses gave the empirical formula $(Fe^{2+}_{0.75}Ca_{0.01}Mn_{0.02}Fe^{3+}_{0.22})_{\Sigma 1.00}(Fe^{3+}_{4.88}Al_{0.04})_{\Sigma 4.92}(PO_4)_4O_{0.11}(OH)_{4.76}{\cdot}6H_2O$. Ferroberaunite is monoclinic, $C2/c$, with $a = 20.8708(3)$, $b = 5.1590(8)$, $c = 19.2263(3)$ Å, $\beta = 93.3186(17)°$, $V = 2066.7(3)$ Å^3 and $Z = 4$. The eight strongest lines in the powder X-ray diffraction pattern are [d_{meas}, Å ($I_{rel.}$, %) (hkl)]: 10.410 (100) (200), 9.606 (14) (002), 7.271 (11) (20$\bar{2}$), 5.203 (4) (400), 3.467 (12) (600), 3.325 (6) (60$\bar{2}$), 3.201 (6) (006), 2.600 (4) (800). The mineral is isostructural with beraunite, redefined recently as $Fe^{3+}_6(PO_4)_4O(OH)_4{\cdot}6H_2O$.

Keywords: ferroberaunite, new mineral, phosphate, crystal structure, Raman spectroscopy, XPS spectroscopy, Cornwall

(Received 10 January 2022; accepted 7 February 2022; Accepted Manuscript published online: 16 February 2022; Associate Editor: Elena Zhitova)

Introduction

The mineral beraunite was discovered by Breithaupt (1840, 1841) on specimens that originated from the Hrbek iron ore mine at Svatá Dobrotivá (Sankt Benigna) in Central Bohemia, nowadays the Czech Republic. In the decades following, similar hydrated basic iron phosphates were classified as either red beraunite or green dufrénite ('kraurite'). The development of structural analysis by X-ray diffraction since the beginning of the 20th Century resulted in a significant advance in mineralogy. Systematic study of basic phosphates has shown that some green acicular phases considered as dufrénite have an X-ray pattern identical to the mineral beraunite. Chemical analyses of this green beraunite have proven the presence of significant amounts of divalent iron, which has not been reported previously (Frondel, 1949; Moore, 1970). Both mixed-valence and trivalent beraunites were considered to be varieties of the same mineral species. On the basis of the refinement of the crystal structure, Moore and Kampf (1992) proposed a trivial name (i.e. 'beraunite') for the 'reduced' (green), and the same name with the prefix 'oxy-' (i.e. 'oxyberaunite') for 'oxidised' (red/orange) end-members. These observations were followed up by Chukanov *et al.* (2017), who introduced the name 'eleonorite' for the Fe^{3+} dominant phase and suggested using the name beraunite for the mixed-valence iron end-member.

A recent investigation of the original 'beraunite' material stored in collections of the Freiberg University of Mining and Technology, Germany, proved the identity of this mineral with 'eleonorite'. The name 'eleonorite' has been discredited and the formula of beraunite as $Fe^{3+}_6(PO_4)_4O(OH)_4{\cdot}6H_2O$ was approved by proposal IMA 21-D (Miyawaki *et al.*, 2021) of the Commission on New Minerals, Nomenclature and Classification of the International Mineralogical Association (IMA–CNMNC). To avoid duplicity of the mineral name 'beraunite', the end-member with mixed iron valence has been redefined and renamed. From several studied specimens of green-coloured 'beraunites' (e.g. Blaton, Belgium; Svappavaara, Sweden; Hagendorf-Süd, Germany; Krásno and Morašice, Czech Republic), a sample originating from the Gravel Hill mine,

***Author for correspondence:** Jaromír Tvrdý, Email: jt.geologie@gmail.com
Cite this article: Tvrdý J., Plášil J., Vrtiška L., Sejkora J., Škoda R., Dolníček Z., Petr M. and Veselovský F. (2022) Ferroberaunite, $Fe^{2+}Fe^{3+}_5(PO_4)_4(OH)_5{\cdot}6H_2O$, a mixed-valence iron member of the beraunite series, from the Gravel Hill mine, Perranzabuloe, Cornwall, England. *Mineralogical Magazine* **86**, 363–372. https://doi.org/10.1180/mgm.2022.15

Perranzabuloe, Cornwall, England, was chosen to define ferroberaunite. The reasons are excellent single-crystal X-ray data and the relative chemical purity, i.e. the absence of common isomorphic elements such as Al, Zn and Mn.

The mineral is named ferroberaunite after its composition, i.e. the presence of divalent iron in the *M*1 site of the beraunite structure. The name is consistent with the name of the related mineral zincoberaunite, $ZnFe_5^{3+}(PO_4)_4(OH)_5{\cdot}6H_2O$ (Chukanov *et al.*, 2016). The name ferroberaunite was previously used by Golley and Williams (1995) as a beraunite variety name referring to minerals from the Gravel Hill mine. The mineral symbol based on Warr (2021) is Fbru. The mineral, mineral name and mineral symbol were approved by the IMA–CNMNC prior to publication (|IMA2021-036, Tvrdý *et al.*, 2021). The holotype specimen is housed in the mineralogical collection of the Department of Mineralogy and Petrology of the National Museum, Prague, Czech Republic, catalogue number P1P 11/2021.

Occurrence

The ferroberaunite specimen was collected around 2016 in the abandoned Gravel Hill mine, Perranzabuloe, Cornwall, England (50°22'27.0"N, 5°08'42.0"W). The mining at the Gravel Hill mine (formerly known as Penhale Iron mine, or Cliff Iron mine) culminated in the 18–19th Centuries. The mine was located on the western end of the Perran Iron Lode, represented here by two layers of oxide iron ore deposited in sedimentary rocks of the Middle Devonian age. The layers are 5 and 13 m thick and are separated by a 14 m thick barren horizon. The ores were formed by oxidation of primary siderite, which is probably of a low-temperature sedimentary- or volcanic-exhalative origin (Scrivener *et al.*, 2006). The total production of the mine is estimated at more than 35,000 tons of iron ore (Cantrill *et al.*, 1919; Dines, 1956).

Ferroberaunite crystallised under supergene conditions in fissures and cavities of 'limonite' iron ore. Cavities are up to 8 cm × 4 cm × 1 cm in size and are often coated with manganese oxides. The occurrence has been known since 1986 and is reported to have been the first discovery of beraunite/ferroberaunite and strunzite/ferrostrunzite in Great Britain (Weiss, 1989, 2019). Other phosphate minerals reported to occur at the Gravel Hill mine include corkite, diadochite, fluorapatite, phosphosiderite, rockbridgeite, strengite and whitmoreite (Golley and Williams, 1995).

Appearance, physical properties and optical data

The holotype specimen of ferroberaunite is a 4 cm × 4 cm × 3 cm fragment of fine-grained limonitised quartz of ochre-brown colour. No associated phosphates are present.

On the holotype specimen, ferroberaunite occurs in long prismatic, acicular to lath-like crystals up to 400 μm long, growing irregularly on matrix or forming radial to spherical aggregates; parallel intergrowths are common (Figs 1, 2). The crystals are flattened on {100} and elongated along the **b** axis, with wedge-shaped terminations. The crystal forms assigned to the orientation given by Marzoni Fecia di Cossato *et al.* (1989) for manganese-rich beraunite from Mangualde, Portugal, comparing with our observation of morphology and powder X-ray diffraction data are {100}, {201}, {20$\bar{1}$}, {112} and {$\bar{1}1\bar{2}$} (Fig. 3); twinning is on {100} (from morphology).

The mineral is dark green to olive green, transparent to translucent, with a pale olive-green streak; the mineral is non-fluorescent. It has a vitreous lustre, pearly on cleavages. The cleavage is very good parallel to {100}. The crystals are brittle with uneven fracture; the Mohs hardness is assumed to be 3–4. The density 2.94(2) g·cm^{-3} was determined by the flotation method using the Mohr-Westphal scale and two different mixtures of liquids (diiodomethane and acetone; 1,1,2,2-tetrabromoethane and dioxane). The calculated density based on the empirical formula and unit-cell parameters from single-crystal diffraction is 2.907 g·cm^{-3}. Ferroberaunite dissolves easily in HCl (35%), slowly in H_3PO_4 (85%); it does not dissolve in HNO_3 (65%; room temperature; 24 hours observation).

The optical properties of ferroberaunite were measured at a wavelength of 589 nm using a microrefractometer spindle-stage (Department of Geological Sciences, Masaryk University in Brno). The extinction is parallel to the elongation. The mineral is biaxial (–), $\alpha = 1.736(2)$, $\beta = 1.765(3)$, $\gamma = 1.786(5)$, $2V_{meas.} = 68(3)°$ and $2V_{calc.} = 79°$. Dispersion of optical axes is strong, $r > v$. The orientation is $Y = \mathbf{b}$; $X \approx \mathbf{a}$, $Z \approx \mathbf{c}$. Pleochroism is strong, X = bluish green >> Z = green > Y = yellow. The Gladstone–Dale

Fig. 1. Ferroberaunite in olive-green acicular crystals on 'limonite' matrix; holotype specimen (catalogue number P1P 11/2021). FOV 2 mm across. Photo by L. Vrtiška.

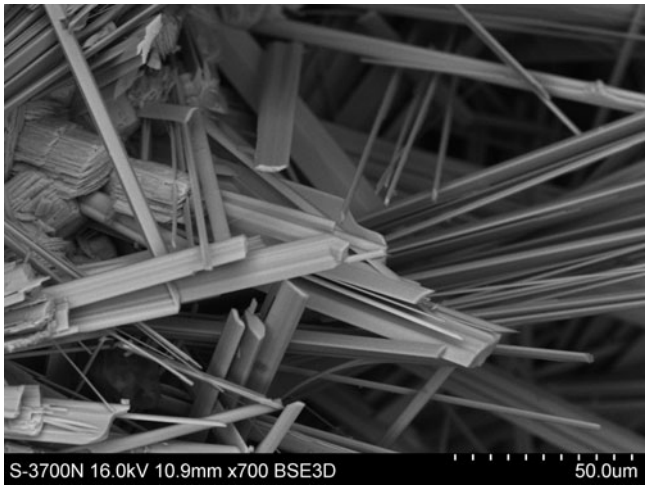

Fig. 2. Scanning electron microscopy image of the holotype ferroberaunite specimen. Thin needles and packets of multiple twins also occur among the predominant lath-like crystals. Graphic scale. Photo by L. Vrtiška.

https://doi.org/10.1180/mgm.2022.15 Published online by Cambridge University Press

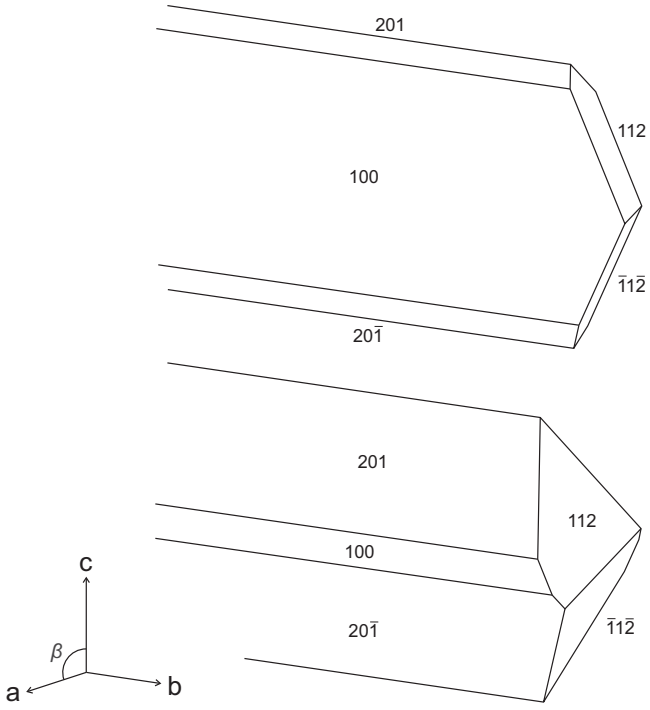

Fig. 3. Drawing of flattened (top) and columnar (bottom) ferroberaunite crystals.

compatibility using revised constants in table 7 of Mandarino (1981) is excellent; 0.038 for empirical formula and measured density, and 0.027 for empirical formula and density calculated from the single-crystal cell.

Chemical composition

The composition of ferroberaunite was determined on polished and carbon-coated fragments mounted in an epoxy cylinder using a Cameca SX 100 electron microprobe (Department of Mineralogy and Petrology, National Museum Prague). The instrument was operated in wavelength-dispersive mode at an accelerating voltage of 15 kV, beam current of 5 nA, with a beam diameter of 7 µm. The following X-ray lines and standards were selected; *Kα* lines: P, Ca (apatite), Al (Al_2O_3), Mn (rhodonite) and Fe (hematite). Contents of Na, Mg, Si, K, S, Cl, Ti, Co, V, Cu, F, Cr, N, As, Mo, Sn, Ba, Y, W, Bi, U, Pb and Th were below detection limits (~0.05–0.10 wt.%). Counting times were 10–20 s on peak and half of this time for each background position. The raw intensities were converted to the concentrations automatically using the *PAP* (Pouchou and Pichoir, 1985) matrix-correction procedure.

Analytical data for ferroberaunite are given in Table 1. In addition to iron, the holotype specimen contains minor amounts of Al (0.04 atoms per formula unit), Mn (0.02 apfu) and Ca (0.01 apfu). The empirical formula of ferroberaunite calculated on the basis of P = 4 apfu is: $(Fe^{2+}_{0.75}Ca_{0.01}Mn_{0.02}Fe^{3+}_{0.22})_{\Sigma 1.00}(Fe^{3+}_{4.88}Al_{0.04})_{\Sigma 4.92}(PO_4)_4O_{0.11}(OH)_{4.76}{\cdot}6H_2O$. The ideal formula is $Fe^{2+}Fe^{3+}_5(PO_4)_4(OH)_5{\cdot}6H_2O$, which requires FeO 7.91, Fe_2O_3 43.97, P_2O_5 31.26, H_2O 16.86, total 100 wt.%.

Table 1. Chemical data (in wt %) for ferroberaunite ($N = 6$).

Constituent	Mean	Range	S.D. (σ)	Reference material
FeO*	6.00	5.88–6.07	0.06	–
CaO	0.05	0.00–0.12	0.05	Apatite
MnO	0.16	0.00–0.32	0.10	Rhodonite
Fe_2O_3	45.38	44.63–45.94	0.48	Hematite
Al_2O_3	0.21	0.14–0.25	0.04	Al_2O_3
P_2O_5	31.60	30.98–31.96	0.33	Apatite
H_2O**	16.80	16.63–17.02	0.15	–
Total	100.20			

* FeO calculated based on an assumption of 0.75 apfu Fe^{2+} in the *M*1 position.
** H_2O could not be analysed directly because of the minute amount of material available, and was calculated on the basis of 6 H_2O, from the ideal composition of beraunite-related minerals and on the basis of neutral charge balance (OH).
S.D. – standard deviation.

Raman spectroscopy

The Raman spectrum of ferroberaunite (Fig. 4) was collected in the range 3600–50 cm^{-1} using a DXR dispersive Raman Spectrometer (Thermo Scientific) mounted on a confocal Olympus microscope. The Raman signal was excited by an unpolarised 633 nm He–Ne gas laser and detected by a CCD detector (size 1650 × 200 pixels, Peltier cooled to –60°C, quantum efficiency 50% and dynamic range 360–1100 nm). The experimental parameters were: 100× objective, 10 s exposure time, 1800 exposures, 50 µm pinhole spectrograph aperture and 3 mW laser power level (estimated resolution 6.4–13.3 cm^{-1}, estimated spot size 0.8 µm). The spectra were acquired repeatedly from different grains in order to obtain a representative spectrum with the best signal-to-noise ratio. The possible thermal damage of the measured point was excluded by visual inspection of the exposed surface after measurement, observing possible decay of spectral features at the start of excitation, and checking for thermal downshift of Raman lines. The instrument was set up by a software-controlled calibration procedure using multiple neon emission lines (wavelength calibration), multiple polystyrene Raman bands (laser-frequency calibration) and standardised white-light sources (intensity calibration). Spectral manipulations were performed using the *Omnic 9* software (Thermo Scientific).

The Raman spectrum shows bands induced by vibrations of OH units and water molecules, as well as $(PO_4)^{3-}$ tetrahedral and Fe–O octahedral units, similar to other hydrated hydroxyphosphates (e.g. Frost *et al.*, 2014, 2016). The high-energy region over 1300 cm^{-1} is characterised by vibrations of OH ions and hydrogen-bonded water molecules. There occur two significant bands assigned to the ν O–H stretching (3561 cm^{-1}) and to the H–O–H ν_2 (δ) bending of water molecules (the broad peak at 1613 cm^{-1}). The next group of bands is connected with stretching vibrations of $(PO_4)^{3-}$ units, namely to the ν_3 antisymmetric (maxima at 1137 and 1051 cm^{-1}) and ν_1 symmetric (1014 cm^{-1}) modes. The Raman bands at 681, 624 and 574 cm^{-1} could be attributed to ν_4 (δ) $(PO_4)^{3-}$ out-of-plane bending vibrations. Bands of the ν_2 (δ) in-plane bending vibrations of the same unit appear at lower wavelengths (470 and 434 cm^{-1}). Further bands could be attributed to vibrations of Fe-centred octahedra in the crystal structure of ferroberaunite. Bands of Fe–O stretching (most likely at 399–294 cm^{-1}) and O–Fe–O symmetric bending (most likely at 232 and 201 cm^{-1}) overlap with the manifestations of external and lattice vibrations, which continue until the end of the spectrum with the maxima at 232, 201, 128 and 87 cm^{-1}.

X-ray photoelectron spectroscopy

Relative proportions of divalent and trivalent iron were estimated by the X-ray photoelectron spectroscopy (XPS) measurements

https://doi.org/10.1180/mgm.2022.15 Published online by Cambridge University Press

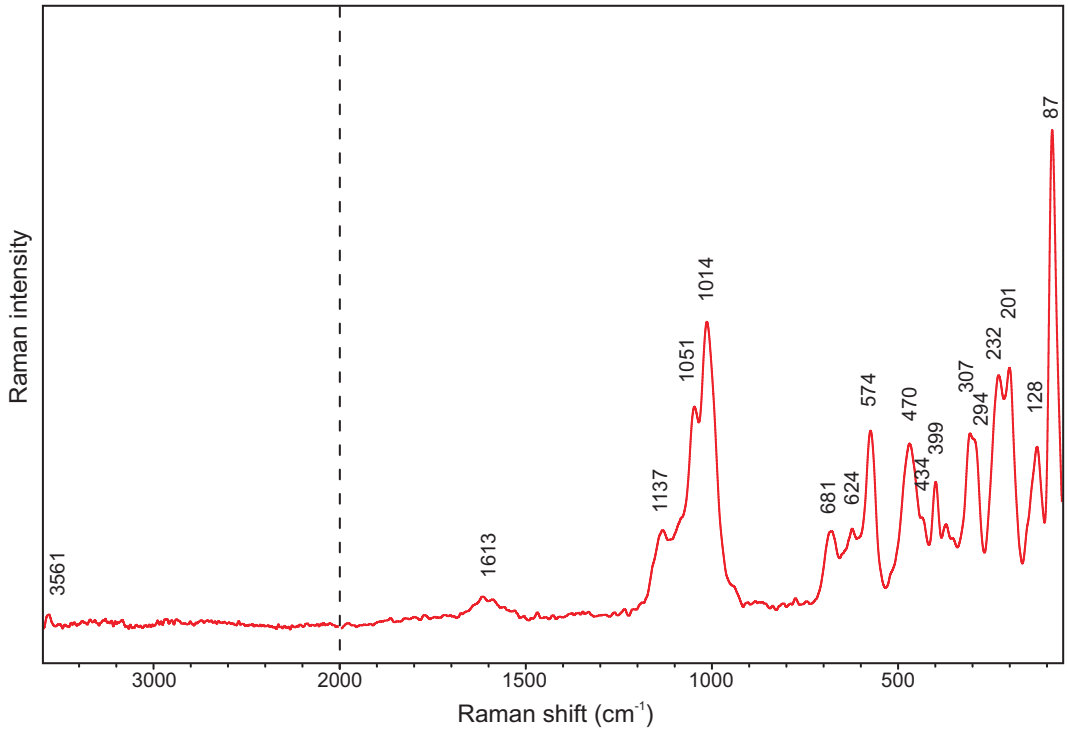

Fig. 4. Raman spectrum of ferroberaunite (split at 2000 cm^{-1}).

carried out with the PHI 5000 VersaProbe II XPS system (Physical Electronics; Regional Centre of Advanced Technologies and Materials, Palacký University Olomouc) using a monochromatic Al*K*α source (15 kV and 50 W) and photon energy of 1486.7 eV. All the spectra were measured in a vacuum of 1.1×10^{-7} Pa and at a temperature of 21°C. The analysed area on the sample was a spot 100 µm in diameter. The survey spectra were measured with a pass energy of 187.850 eV and electronvolt step of 0.8 eV, whereas the high-resolution spectra were measured with a pass energy of 23.500 eV and electronvolt step of 0.2 eV. Dual-beam charge compensation was used for all measurements. All binding energy values were referenced to the carbon peak C1s at 284.80 eV.

Table 2. Estimation of a relative content of Fe^{2+} based on the area of the peak Fe $2p_{3/2}(1)$.

Mineral, locality, ideal formula	Peak	Binding energy (eV)	Area (%)	Fe^{2+} (%)
Ferroberaunite*	(1)	708.6	2.2	12
Gravel Hill mine, Cornwall, UK	(2)	710.8	76.1	
$Fe^{2+}Fe^{3+}_5(PO_4)_4(OH)_5{\cdot}6H_2O$	(3) shake-up	713.0	21.8	
Beraunite**	(1)	709.4	1.2	0
Hrbek mine, Bohemia, Czech Republic	(2)	711.7	62.9	
$Fe^{3+}_6(PO_4)_4O(OH)_4{\cdot}6H_2O$	(3) shake-up	713.5	35.9	
Vivianite***	(1)	709.3	8.8	92
Roșia Poieni, Alba, Romania	(2)	711.0	59.3	
$Fe^{2+}_3(PO_4)_2{\cdot}8H_2O$	(3) shake-up	713.8	31.9	
Childrenite	(1)	709.0	9.5	100
George & Charlotte mine, Devon, UK	(2)	710.9	64.9	
$Fe^{2+}Al(PO_4)(OH)_2{\cdot}H_2O$	(3) shake-up	714.0	25.6	

* Holotype specimen; ** neotype specimen (sample NM; Vrtiška *et al.*, 2022); *** probably partly oxidised.

Data were analysed with *MultiPak* (Ulvac-PHI, Inc.) software version 9.9.0.8 using Gaussian–Lorentzian function with iterated *Shirley* routine background subtraction (Shirley, 1972).

Generally, p orbitals exhibit spin-orbit splitting in XPS. The spin-orbit splitting is projected as a doublet in the XPS spectrum (Briggs, 2003). In the Fe 2p region, there is significant splitting of the Fe $2p_{3/2}$ and Fe $2p_{1/2}$ components (~13 eV) with the ratio 2:1, respectively. Another spectral features in this region are shake-up lines caused by a finite probability that the ion will be left in an excited state a few electronvolts above the ground state. This leads to the formation of satellite peaks (Moulder *et al.*, 1995). As the fitting procedure of the Fe 2p region is very complex, the simplifying practice used for the natural mineral phases by Kloprogge and Wood (2020) was chosen.

To estimate the valence states of iron, an empirical approach comparing Fe $2p_{3/2}$ spectra with standards was used, which avoids having to describe the peak shapes analytically (e.g. Rhodes, 2021). Holotype ferroberaunite was compared with the spectra of beraunite, vivianite and childrenite (Table 2). High-resolution spectra for the 707–717 eV binding energy section decomposed to three main peaks for Fe $2p_{3/2}$ are shown in Fig. 5. Although the determination of the iron oxidation state is complicated, the ratio Fe^{2+} : (Fe^{2+}+Fe^{3+}) can be estimated from the relative area of the peak Fe $2p_{3/2}(1)$ and the corresponding regression curve. The observed value of ~12% Fe^{2+} corresponds to 0.72 apfu in the ferroberaunite formula.

X-ray diffraction data and crystal structure

Powder X-ray diffraction data for ferroberaunite were recorded at room temperature using a Bruker D8 Advance diffractometer equipped with solid-state LynxEye detector and secondary monochromator producing Cu*K*α radiation (Department of Mineralogy

https://doi.org/10.1180/mgm.2022.15 Published online by Cambridge University Press

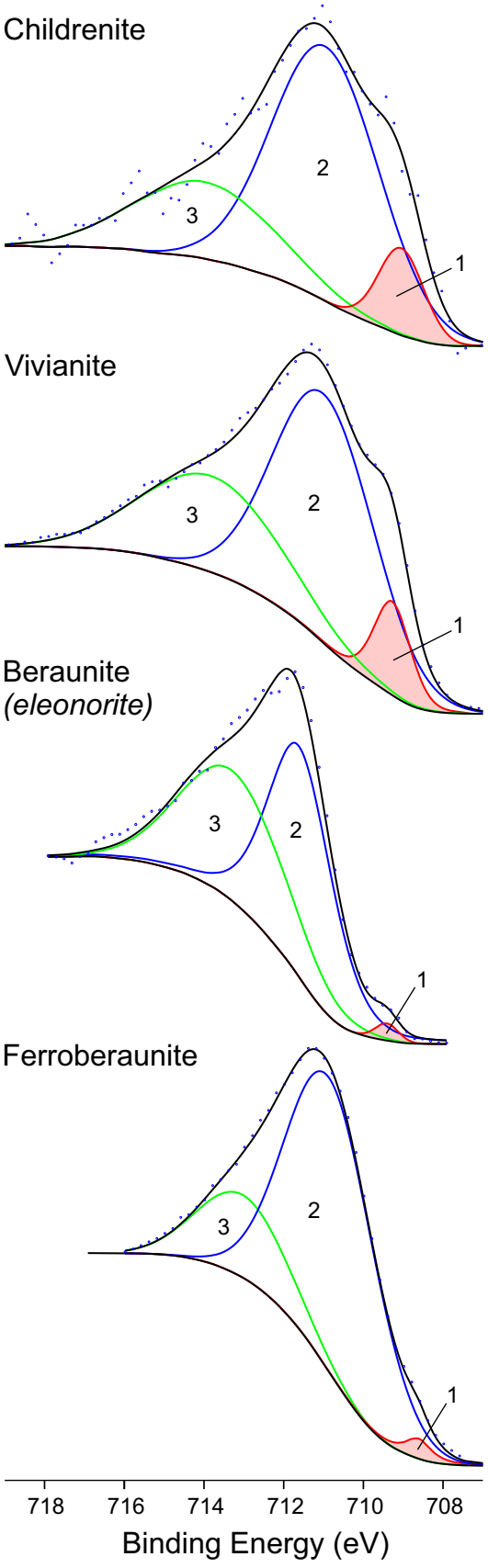

Fig. 5. Comparison of high resolution Fe $2p_{3/2}$ XPS spectrum of ferroberaunite with patterns of ferric (beraunite/'eleonorite') and ferrous phosphates (vivianite and childrenite). The spectra are vertically shifted. The numbering of peaks corresponds to Table 2; the peaks $Fe2p_{3/2}(1)$ used to estimate a relative content of Fe^{2+} are highlighted.

Table 3. Powder diffraction data (d in Å) for ferroberaunite*.

I_{meas}	I_{calc}	d_{meas}	d_{calc}	h	k	l
100.0	**100.0**	**10.4096**	10.3993	2	0	0
14.2	**41.6**	**9.6065**	9.6001	0	0	2
11.3	**30.7**	**7.2709**	7.2656	2	0	$\bar{2}$
4.2	2.8	5.2035	5.1996	4	0	0
3.3	32.3	4.8252	4.8265	1	1	1
1.1	5.8	4.4517	4.4570	2	0	$\bar{4}$
1.3	16.2	4.4155	4.4128	1	1	2
2.0	11.5	3.7531	3.7529	3	1	2
0.7	11.0	3.4881	3.4885	1	1	$\bar{4}$
12.0	**12.0**	**3.4675**	3.4664	6	0	0
0.4	11.8	3.4161	3.4213	3	1	3
6.2	**3.6**	**3.3253**	3.3221	6	0	$\bar{2}$
3.3	4.3	3.2421	3.2375	5	1	0
5.8	**11.2**	**3.2015**	3.2000	0	0	6
0.3	11.0	3.1749	3.1692	5	1	1
1.1	5.2	3.1117	3.1093	2	0	$\bar{6}$
2.5	33.3	3.0821	3.0819	3	1	4
0.7	1.8	2.8917	2.8904	6	0	$\bar{4}$
1.1	1.1	2.7992	2.7982	4	0	$\bar{6}$
1.5	9.7	2.7405	2.7416	5	1	$\bar{4}$
2.6	8.5	2.7135	2.7131	1	1	$\bar{6}$
3.8	5.5	2.5997	2.5998	8	0	0
0.7	4.0	2.5738	2.5781	0	2	0
0.7	4.4	2.5738	2.5744	7	1	0
1.1	3.7	2.4294	2.4308	7	1	$\bar{3}$
0.7	3.2	2.4141	2.4133	2	2	2
1.6	4.0	2.3115	2.3098	4	2	0
1.3	2.5	2.2278	2.2285	4	0	$\bar{8}$
1.2	9.9	2.1086	2.1077	3	1	$\bar{8}$
1.4	2.1	2.0793	2.0799	10	0	0
1.1	6.2	2.0085	2.0081	6	2	2
0.8	9.3	1.9239	1.9240	6	2	$\bar{4}$
0.7	3.2	1.7212	1.7222	6	0	$\overline{10}$
2.5	2.8	1.6888	1.6887	12	0	2
0.8	1.2	1.6618	1.6611	12	0	$\bar{4}$
1.0	9.4	1.6185	1.6188	10	2	0
0.4	1.3	1.5672	1.5671	1	3	$\bar{5}$
0.5	1.2	1.4847	1.4856	14	0	0

*The strongest peaks are reported in bold.
a = 20.833(4) Å, b = 5.1562(13) Å, c = 19.232(7) Å, β = 93.30(4)° and V = 2062.5(9) Å^3.

Table 4. Details for the data collection and refinement of the structure of ferroberaunite.

Crystal data	
Chemical formula	$Fe_6H_{17}O_{27}P_4$
M_r	908.1
Crystal system, space group	Monoclinic, $C2/c$
Temperature (K)	298
a, b, c (Å)	20.8708(3), 5.1590(8), 19.2263(3)
β (°)	93.3186(17)
V (Å^3)	2066.7(3)
Z	4
Radiation type	Mo $K\alpha$
μ (mm^{-1})	4.54
Data collection	
Crystal size (mm)	0.089 × 0.014 × 0.013
Diffractometer	Rigaku SuperNova CCD
Absorption correction	Empirical (multi-scan), CrysAlis
T_{min}, T_{max}	0.738, 1.000
No. of measured, independent and observed [$I > 3\sigma(I)$] reflections	18965, 2506, 2301
R_{int}	0.0296
$(\sin\theta/\lambda)_{max}$ (Å^{-1})	0.6733
Refinement	
$R[F^2 > 3\sigma(F^2)]$, $wR(F^2)$, S	0.0202, 0.0652, 1.54
No. of reflections	2506
No. of parameters	195
No. of restraints	10
H-atom treatment	H atoms treated by a mixture of independent and constrained refinement
$\Delta\rho_{max}$, $\Delta\rho_{min}$ (e$^-$ Å^{-3})	0.30, −0.56

https://doi.org/10.1180/mgm.2022.15 Published online by Cambridge University Press

Table 5. Atom coordinates and displacement parameters (as isotropic or equivalent; in Å^2) for the structure of ferroberaunite.

Atom	*Wyckoff*	*x*/*a*	*y*/*b*	*z*/*c*	U_{iso}*/U_{eq}
Fe1(*M1*)	4*a*	½	½	½	0.00962(12)
Fe2(*M4*)	8*f*	0.391901(14)	0.53696(6)	0.585364(15)	0.00917(9)
Fe3(*M3*)	8*f*	0.544145(13)	0.78095(6)	0.672652(15)	0.00882(9)
Fe4(*M2*)	4*d*	¼	¼	½	0.01053(12)
P1	8*f*	0.60515(2)	0.97529(10)	0.52421(3)	0.00709(14)
P2	8*f*	0.40725(3)	1.04456(10)	0.68178(3)	0.00819(15)
O1	8*f*	0.57679(7)	1.2342(3)	0.49702(8)	0.0122(4)
O2	8*f*	0.67768(7)	0.9840(3)	0.51606(8)	0.0114(4)
O3	4*e*	½	0.6129(4)	¾	0.0142(6)
O4	8*f*	0.57518(7)	0.7503(3)	0.48031(8)	0.0115(4)
O5	8*f*	0.49277(7)	0.5406(3)	0.60748(8)	0.0121(4)
O6	8*f*	0.47887(7)	1.0511(3)	0.66704(8)	0.0126(4)
O7	8*f*	0.39947(7)	0.9889(3)	0.75910(8)	0.0148(4)
O8	8*f*	0.37049(7)	0.8419(3)	0.63714(8)	0.0129(4)
O9	8*f*	0.59099(8)	0.9420(3)	0.60010(8)	0.0155(4)
O10	8*f*	0.37842(7)	1.3116(3)	0.66419(8)	0.0123(4)
O11	8*f*	0.30760(7)	0.5228(3)	0.53742(8)	0.0130(4)
O12	8*f*	0.25248(8)	0.4133(3)	0.40119(8)	0.0181(5)
O13	8*f*	0.61512(9)	0.4862(3)	0.68038(11)	0.0247(5)
O14	8*f*	0.26908(10)	0.1399(5)	0.28417(11)	0.0385(7)
H1o14	8*f*	0.2475(14)	−0.018(4)	0.2797(18)	0.0462*
H1o5	8*f*	0.4976(11)	0.370(3)	0.6226(12)	0.0145*
H1o12	8*f*	0.2131(8)	0.496(4)	0.3918(12)	0.0217*
H1o11	8*f*	0.3007(12)	0.681(3)	0.5168(12)	0.0156*
H1o13	8*f*	0.6376(12)	0.465(4)	0.6407(10)	0.0296*
H2o12	8*f*	0.2550(10)	0.290(4)	0.3666(10)	0.0217*
H2o13	8*f*	0.6181(13)	0.328(3)	0.7028(11)	0.0296*
H1o3	4*e*	½	0.434616	¾	0.0170*
H2o14	8*f*	0.3099(9)	0.078(6)	0.2741(17)	0.0462*

M1–*M4* denotes metal cation site labelling, according to Moore and Kampf (1992).

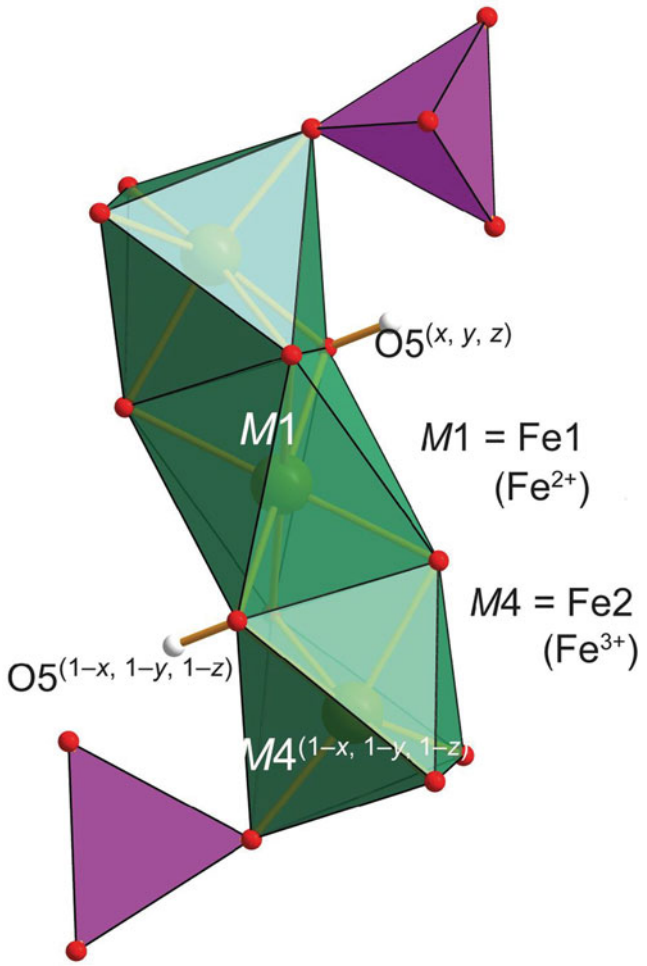

Fig. 6. Octahedral trimer in ferroberaunite. *M*1 is occupied by Fe^{2+} and *M*4 by Fe^{3+}. P tetrahedrons are purple and H atoms grey.

and Petrology, National Museum, Prague). The instrument was operating at 40 kV and 40 mA. In order to minimise the background, the powder samples were placed (without any liquid) on the surface of a flat silicon wafer. The powder pattern was collected in the Bragg–Brentano geometry in the range 3–70°2θ, step 0.01° and counting time of 20 s per step (total duration of the experiment ≈ 30 hours). The positions and intensities of diffractions were found and refined using the Pearson VII profile-shape function of the *ZDS* program package (Ondruš, 1993). Powder diffraction data are given in Table 3; the unit-cell parameters were refined by the least-squares algorithm implemented by

Table 6. Selected interatomic distances (in Å) and polyhedral measures for ferroberaunite.

Fe1–O1^{ii}	2.1125(15)	Fe2–O1^{iii}	2.1093(16)	Fe3–O3	1.9927(10)
Fe1–O1^{iii}	2.1125(15)	Fe2–O4^{i}	2.0888(16)	Fe3–O5	2.0253(15)
Fe1–O4	2.0836(15)	Fe2–O5	2.1236(15)	Fe3–O6	1.9476(16)
Fe1–O4^{i}	2.0836(15)	Fe2–O8	1.9280(16)	Fe3–O7^{iv}	2.0196(15)
Fe1–O5	2.0912(15)	Fe2–O10^{ii}	1.9435(16)	Fe3–O9	1.9362(17)
Fe1–O5^{i}	2.0912(15)	Fe2–O11	1.9398(15)	Fe3–O13	2.1220(18)
<Fe1–Φ>	2.096	<Fe2–Φ>	2.022	<Fe3–Φ>	2.007
$V_{Fe1Φ}$	11.64 Å^3	$V_{Fe2\_1Φ}$	10.75 Å^3	$V_{Fe2\_2Φ}$	10.74 Å^3
$ECoN_{Fe1Φ}$	5.993	$ECoN_{Fe2\_1Φ}$	5.564	$ECoN_{Fe2\_2Φ}$	5.787
$Distortion_{Fe1Φ}$	0.340	$Distortion_{Fe2Φ}$	17.979	$Distortion_{Fe3Φ}$	9.336
Fe4–O2^{v}	1.9710(15)	P1–O1	1.5401(16)	P2–O6	1.5378(16)
Fe4–O2^{i}	1.9710(15)	P1–O2	1.5315(15)	P2–O7	1.5317(17)
Fe4–O11	1.9604(15)	P1–O4	1.5459(16)	P2–O8	1.5306(16)
Fe4–O11^{vi}	1.9604(15)	P1–O9	1.5153(17)	P2–O10	1.5331(17)
Fe4–O12	2.0816(15)	<P1–Φ>	1.533	<P2–Φ>	1.533
Fe4–O12^{vi}	2.0816(15)				
<Fe4–Φ>	2.004				
$V_{Fe4Φ}$	10.71 Å^3				
$ECoN_{Fe4Φ}$	5.840				
$Distortion_{Fe4Φ}$	7.432				

Symmetry codes: (i) –*x*+1, –*y*+1, –*z*+1; (ii) *x*, *y*–1, *z*; (iii) –*x*+1, –*y*+2, –*z*+1; (iv) –*x*+1, *y*, –*z*+3/2; (v) *x*–½, *y*–½, *z*; (vi) –*x*+½, –*y*+½, –*z*+1. *ECoN* – effective coordination number (Hoppe, 1979); *distortion* – octahedral distortion (Brown and Shannon, 1973).

https://doi.org/10.1180/mgm.2022.15 Published online by Cambridge University Press

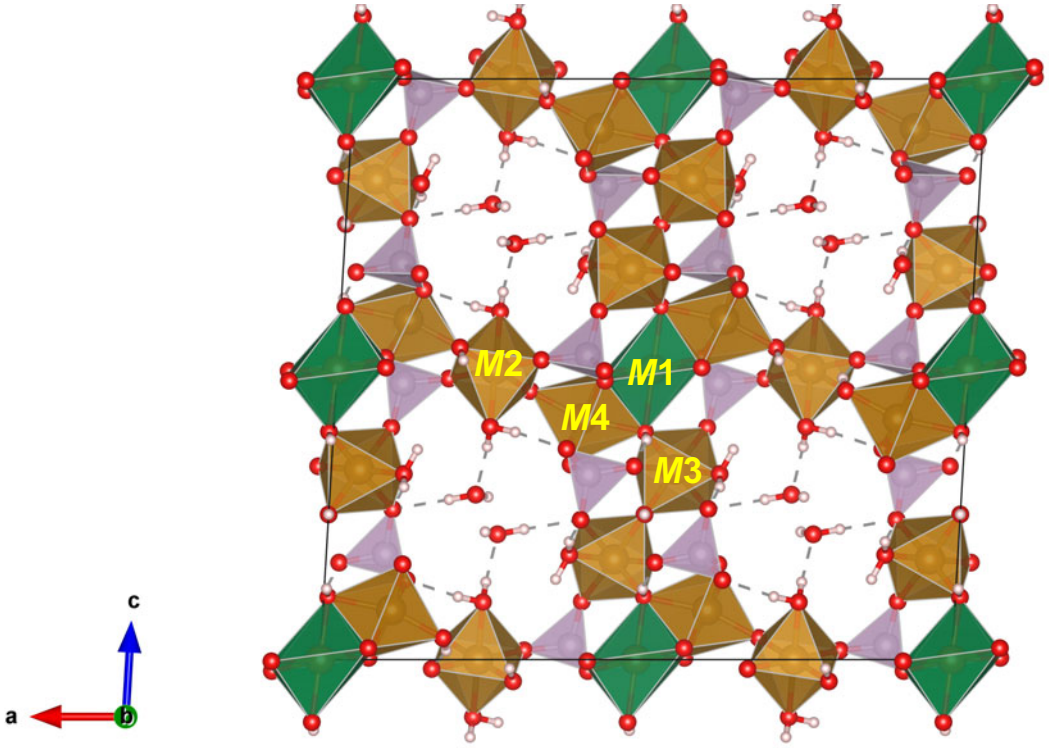

Fig. 7. Crystal structure of ferroberaunite viewed perpendicular to the crystal elongation. The heteropolyhedral slabs are connected by the *M*2-octahedra; water molecules located in channels are hydrogen-bonded (dashed lines). P tetrahedrons are purple, O atoms red and H atoms grey. The unit cell edges are outlined in black.

Burnham (1962) as: $a = 20.833(4)$ Å, $b = 5.1562(13)$ Å, $c = 19.232(7)$ Å, $\beta = 93.30(4)°$ and $V = 2062.5(9)$ Å^3.

For the single-crystal diffraction experiment, a long-prismatic crystal was separated under a polarising microscope and mounted on a glass fibre. The diffraction experiment (see Table 4 for details) was performed at room temperature with a Rigaku SuperNova single-crystal diffractometer equipped with the Atlas S2 CCD detector and a microfocus Mo*K*α source (Institute of Physics, CAS, Prague). Data reduction was performed using *CrysAlisPro* Version 1.171.39.46 (Rigaku, 2019). The data were corrected for the Lorentz factor and polarisation effects. An absorption correction (empirical scaling using spherical harmonics) was applied in *Jana2020* (Petříček *et al.*, 2020). A single-crystal X-ray experiment revealed a monoclinic unit cell: $a = 20.8708(3)$, $b = 5.1590(8)$, $c = 19.2263(3)$ Å, $\beta = 93.3186(17)°$, $V = 2066.7(3)$ Å^3 and $Z = 4$.

The structure of ferroberaunite was solved from the X-ray data using the intrinsic phasing algorithm of the *SHELXT* program (Sheldrick, 2015) in the monoclinic space-group *C*2/*c*. A centrosymmetric space-group was indicated from the reflection statistics (observed, $|E^2-1| = 1.006$; expected centrosymmetric = 0.968 *vs.* non-centrosymmetric 0.736). The refinement was performed using the full-matrix least-squares algorithm of the *Jana2020* program (Petříček *et al.*, 2020). It revealed the same general model as provided for the beraunite-related structures (Fanfani and Zanazzi, 1967; Moore and Kampf, 1992; Chukanov *et al.*, 2017; Aksenov *et al.*, 2018; Tvrdý *et al.*, 2020). The refinement converged smoothly, including H-atom sites located by Fourier syntheses (H atoms refined using soft constrains on the O–H distances and U_{iso} of the H atoms were set at 1.2 times that of the corresponding donor O atom), to the final $R = 0.0203$ for 2301 unique reflections of $I > 3\sigma(I)$ with a goodness of fit = 1.35; the highest peak that resides in the electron density was 0.37 e$^-$ Å^{-3}, only. The details for the refinement are given in Table 4. Atom coordinates, atomic displacement parameters and site occupancies are given in Table 5, selected interatomic distances in Table 6 and bond-valence analysis in Table 7. The crystallographic information files have been deposited with the Principal Editor of *Mineralogical Magazine* and are available as Supplementary material (see below).

Table 7. Bond-valence analysis for the structure of ferroberaunite (values in valence units, vu).*

	Fe1	Fe2	Fe3	Fe4	P1	P2	ΣBV–H	ΣBV+H
O1	0.36$^{\times2\downarrow}$	0.39			1.23		1.98	1.98
O2				0.57$^{\times2\downarrow}$	1.26		1.83	1.93
O3(OH)			0.53				1.07	2.06
O4	0.39$^{\times2\downarrow}$	0.41			1.22		2.01	2.01
O5(OH)	0.38$^{\times2\downarrow}$	0.37	0.49				1.24	2.18
O6			0.60			1.24	1.84	1.97
O7			0.49			1.26	1.75	1.96
O8		0.64				1.26	1.90	1.90
O9			0.62		1.31		1.94	1.93
O10		0.61				1.26	1.88	1.88
O11(OH)		0.62		0.58$^{\times2\downarrow}$			1.20	2.17
O12(H_2O)				0.42$^{\times2\downarrow}$			0.42	2.34
O13(H_2O)			0.37				0.37	2.31
O14(H_2O)							0.00	2.09
ΣBV	2.25	3.03	3.11	3.13	5.02	5.02		

*Bond-valence parameters were taken from Gagné and Hawthorne (2015). ΣBV–H = summation of bond valences without considering H bonds; ΣBV+H = summation of bond valences with H bonds considered.

https://doi.org/10.1180/mgm.2022.15 Published online by Cambridge University Press

Table 8. Comparative data for ferroberaunite and related minerals; unit-cell parameters on the basis of single-crystal data.

Mineral	Ferroberaunite	Beraunite	Zincoberaunite	Tvrdýite
Mineral symbol	Fbru	Bru	Zbru	Tvr
Idealised formula	$Fe^{2+}Fe^{3+}_5(PO_4)_4(OH)_5{\cdot}6H_2O$	$Fe^{3+}_6(PO_4)_4O(OH)_4{\cdot}6H_2O$	$ZnFe^{3+}_5(PO_4)_4(OH)_5{\cdot}6H_2O$	$Fe^{2+}Fe^{3+}_2Al_3(PO_4)_4(OH)_5{\cdot}6H_2O$
Site *M*1	Fe^{2+}	Fe^{3+}	Zn	Fe^{2+}
Site *M*4	Fe^{3+}	Fe^{3+}	Fe^{3+}	Fe^{3+}
Sites *M*2+*M*3	Fe^{3+}	Fe^{3+}	Fe^{3+}	Al
Crystal system	Monoclinic	Monoclinic	Monoclinic	Monoclinic
Space group	*C*2/*c*	*Cc*	*C*2/*c*	*C*2/*c*
a (Å)	20.8708(3)	20.6507(6)	20.837(2)	20.564(4)
b (Å)	5.1590(8)	5.1377(2)	5.1624(4)	5.1010(10)
c (Å)	19.2263(3)	19.2152(5)	19.250(1)	18.883(4)
β (°)	93.3186(17)	93.523(2)	93.252(5)	93.68(3)
Volume (Å^3)	2066.7(3)	2034.82(11)	2067.3(3)	1976.7(7)
Z	4	4	4	4
Optical	Biaxial (–)	Biaxial (+)	Biaxial (–)	Biaxial (–)
α	1.736	1.768	1.745	1.650
β	1.765	1.781	1.760	1.671
γ	1.786	>1.805	1.770	1.677
2*V*	68° (meas.) / 71° (calc.)	69° (meas.)	80°	56°
Density	2.907 (calc.)	2.961 (calc.)	2.938 (calc.)	2.834 (calc.)
References	This paper	Vrtiška *et al.* (2022)	Chukanov *et al.* (2016)	Sejkora *et al.* (2016)

Ferroberaunite possesses some structural elements common to basic phosphates of ferrous and ferric iron (Moore, 1969, 1970). Distinct fundamental building blocks are trimers of face-shared *M*1- and *M*4-octahedra, where the inner $[M1O_4(OH1)_2]$-octahedron occupies the 4*a*-site and the outer $[M4O_4(OH1)(OH2)]$-octahedra occupy 8*f*-sites, for the *C*2/*c* structures (Fig. 6). The trimers are further linked *via* two isolated $[P1O_4]$-tetrahedra along the **b** direction. Along the **c** direction they are connected by corner-sharing with $[M3O_3(OH)_2(H_2O)]$-octahedra and $[P2O_4]$-tetrahedra, which results in heteropolyhedral layers (Fig. 7). These layers are then linked *via* *M*2-octahedra forming a framework containing wide channels running parallel to **b** and hosting H_2O. The seven structural blocks of these octahedra (triplets with corner shared octahedra) are referred to as the *h*-clusters by Moore (1969, 1970).

The distinction between beraunite (formerly 'eleonorite'; IMA 21-D, Miyawaki *et al.*, 2021) and ferroberaunite is the occupancy of the *M*1 site. Whereas for beraunite, *M*1 is populated by trivalent iron cation, ferroberaunite contains divalent iron at *M*1. This has been proved unambiguously by the results of the bond-valence analysis (Table 7), consistent with a site occupancy of 75% Fe^{2+} and 25% of Fe^{3+}. The formula of ferroberaunite, reflecting the occupancy of the *M*1 site as suggested by the bond-valence analysis and which is in line with the results from electron microprobe spectroscopy, is $(Fe^{2+}_{0.75}Fe^{3+}_{0.25})Fe^{3+}_5(PO_4)_4(OH)_5(H_2O)_6$; this formula is not electroneutral, having +0.25 charge. The exact mechanism of the charge-balance is probably *via* OH↔O substitution. In the case of ferroberaunite, its resolution is far beyond the capabilities of the current X-ray data. The ideal, electroneutral formula for ferroberaunite is $Fe^{2+}Fe^{3+}_5(PO_4)_4(OH)_5(H_2O)_6$, $Z = 4$ and $D_{calc} = 2.919$ g·cm^{-3}.

Discussion

The crystal structure of minerals of the beraunite–ferroberaunite series has been investigated by several authors. Fanfani and Zanazzi (1967) studied, using the Weissenberg method, a crystal of 'red' beraunite from the Eleonore iron mine near Giessen, Germany. For this sample, the authors determined by microchemical analysis (colorimetric test), somewhat surprisingly, a ratio of divalent to trivalent iron of 1 : 5.9 and a formula corresponding to the present-day ferroberaunite. Nevertheless, the refined bond lengths within the Fe-octahedra unambiguously show iron as trivalent (Fe1 = 2.96 valence units (vu), Fe2 = 3.43 vu, Fe3 = 3.15 vu, Fe4 = 2.99 vu; using bond-valence parameters given for Fe^{3+} by Gagné and Hawthorne, 2015). Subsequently, Moore (1970) published refined unit-cell data derived from a powder image of 'green beraunite' (i.e. ferroberaunite) from the Palermo No. 1 Pegmatite, New Hampshire, USA. In the Mn-rich 'red' beraunite from Mangualde, Portugal, Marzoni Fecia di Cossato *et al.* (1989) hypothesised the presence of exclusively trivalent iron and the dominance of divalent manganese at the *M*2 site; these conclusions were discussed subsequently by Moore and Kampf (1992) and Aksenov *et al.* (2018). In this site, divalent manganese cannot be present, based on refined bond lengths (Mn2 = 2.97 vu; using bond-valence parameters given for Mn^{3+} by Gagné and Hawthorne, 2015), and the rest of the sites assigned to Fe are dominated by trivalent iron (Fe1 = 2.77 vu, ~ 24% Fe^{2+} and 77% Fe^{3+}; Fe3 = 3.10 vu; and Fe4 = 3.01 vu; using bond-valence parameters given by Gagné and Hawthorne, 2015). Moore and Kampf (1992) analysed the published structural data and compared it with new measurements on 'green beraunite' from Mullica Hill, New Jersey, USA. There is little doubt that they analysed what is approved now as ferroberaunite (Fe1 = 2.30 vu, ~70% Fe^{2+} and 30% Fe^{3+}; Fe2 = 3.40 vu; Fe3 = 3.15 vu; Fe4 = 2.99 vu; using bond-valence parameters given by Gagné and Hawthorne, 2015).

Further structural data are later reported by Chukanov *et al.* (2017) for beraunite ('eleonorite') and by Aksenov *et al.* (2018) for Mn-rich beraunite ('eleonorite'). In the case of the sample studied by Aksenov *et al.* (2018), the authors concluded that all octahedral sites are occupied dominantly by trivalent iron, Mn^{2+} is present in an amount of only 0.28 apfu in *M*1 and its excess (~0.3 apfu) is disordered between *M*2–*M*4 sites with different Fe^{3+}: Mn^{2+} ratios.

'Eleonorite', re-established by Chukanov *et al.* (2017), is a mineral with the Fe^{3+} dominating over all the octahedral metal sites in the structure. The structure model of Chukanov *et al.* (2017) corresponds to an average structure of the centrosymmetric

https://doi.org/10.1180/mgm.2022.15 Published online by Cambridge University Press

monoclinic space group $C2/m$. This model comprises a partially occupied OH1 site (50% O and 50% OH). This means there must also be an H site with 50% occupancy. The OH1 site is related to the $M1$-octahedron, which hosts Fe^{3+} in the case of beraunite ('eleonorite' of Chukanov *et al.*, 2017). The structure model for beraunite proposed by Vrtiška *et al.* (2022) adopts a non-centrosymmetric monoclinic space group Cc, with the fully occupied H site linked to the O5_2 site of the $M1$-octahedron, equivalent to the $O5^{(1-x,\ 1-y,\ 1-z)}$ site in ferroberaunite (Fig. 6). Such a model provides a non-averaged structure with one of the vertices of the $M1$-octahedron deprotonated, resulting in the formula $Fe_6^{3+}(PO_4)_4O(OH)_4{\cdot}6H_2O$. In contrast to the centrosymmetric structure of ferroberaunite, $Fe^{2+}Fe_5^{3+}(PO_4)_4O(OH)_5{\cdot}6H_2O$, two of the $M1$-octahedral vertices (represented by the symmetrically related O5 atoms) are linked to H atoms of the OH groups.

Conclusions

The redefinition of beraunite and the approval of the new mineral name ferroberaunite should correctly clarify the status of these structurally and chemically close, but distinct, mineral phases. Ferroberaunite is a Fe^{2+} analogue of zincoberaunite (Zn dominant in the $M1$ site) and beraunite (Fe^{3+} dominant in the $M1$ site), and isostructural with the hydrated iron-aluminium basic phosphate tvrdýite (Table 8). The identification of these minerals is possible only by both chemical and structural analyses. For Fe^{2+}/Fe^{3+} dominant phases, the rule 'dark green ferroberaunite' and 'red-brown beraunite' generally applies.

Supplementary material. To view supplementary material for this article, please visit https://doi.org/10.1180/mgm.2022.15

Acknowledgements. We thank Stuart Mills and editorial board members for handling of the manuscript. The paper benefited from constructive comments of Anthony Kampf, Oleg Siidra and Martin Števko. The work was supported financially by the Ministry of Culture of the Czech Republic (long-term project DKRVO 2019-2023/1.II.d National Museum, 00023272), the Grant Agency of the Masaryk University Brno, Czech Republic (Project MUNI/A/1387/2018), the Czech Ministry of Education, Youth and Sports (Project No. SOLID21 CZ.02.1.01/0.0/0.0/16_019/0000760, Institute of Physics ASCR), and Strategic Research Plan of the Czech Geological Survey (DKRVO 2018-2022).

References

Aksenov S.M., Chukanov N.V., Göttlicher J., Hochleitner R., Zarubina E.S. and Rastsvetaeva R.K. (2018) Mn-bearing eleonorite from Hagendorf South pegmatite, Germany: Crystal structure and crystal-chemical relationships with other beraunite-type phosphates. *Zeitschrift für Kristallographie*, **233**, 469–477.

Breithaupt A. (1840) Beraunit, ein neues Glied der Phyllit-Ordnung. *Journal für Praktische Chemie*, **20**, 66–67, Barth Verlag, Leipzig.

Breithaupt A. (1841) *Vollständiges Handbuch der Mineralogie, Volume 2*. Arnoldische Buchhandlung, Dresden and Leipzig, Germany.

Briggs D. (2003) XPS: Basic principles, spectral features and qualitative analysis. Pp. 31–56 in: *Surface Analysis by Auger and X-ray Photoelectron Spectroscopy* (D. Briggs and J.T. Grant, editors). IM Publications, Chichester, UK.

Brown I.D. and Shannon R.D. (1973) Empirical bond-strength–bond-length curves for oxides. *Acta Crystallographica*, **A29**, 266–282.

Burnham C.W. (1962) Lattice constant refinement. *Carnegie Institute Washington Yearbook*, **61**, 132–135.

Cantrill T.C., Sherlock R.L. and Dewey H. (1919) Iron ores. Pp. 61–67 in: *Special Reports On The Mineral Resources Of Great Britain*, Vol. 9. HMSO Publishing, London.

Chukanov N.V., Pekov I.V., Grey I.E., Price J.R., Britvin S.N., Krzhizhanovskaya M.G., Kampf A.R., Dünkel B., Keck E., Belakovskiy D.I. and MacRae C.M. (2016) Zincoberaunite, $ZnFe_5^{3+}(PO_4)_4(OH)_5{\cdot}2H_2O$, a new mineral from the Hagendorf South pegmatite, Germany. *Mineralogy and Petrology*, **111**, 351–361.

Chukanov N.V., Aksenov S.M., Rastsvetaeva R.K., Schäfer C., Pekov I.V., Belakovskiy D.I., Scholz R., de Oliveira L.C.A. and Britvin S.N. (2017) Eleonorite, $Fe_6^{3+}(PO_4)_4O(OH)_4{\cdot}2H_2O$: validation as a mineral species and new data. *Mineralogical Magazine*, **81**, 61–76.

Dines H.G. (1956) *The Metalliferous Mining Region of South-West England, Volume 1*. HMSO Publishing, London [pp. 441–442]

Fanfani L. and Zanazzi P.F. (1967) The crystal structure of beraunite. *Acta Crystallographica*, **22**, 173–181.

Frondel C. (1949) The dufrenite problem. *American Mineralogist*, **34**, 513–540.

Frost R.L., López A., Scholz R., Xi Y. and Lana C. (2014) The molecular structure of the phosphate mineral beraunite $Fe^{2+}Fe_5^{3+}(PO_4)_4(OH)_5.4H_2O$. *Spectrochimica Acta*, **A128**, 408–412.

Frost R.L., Scholz R. and López A. (2016) A Raman and infrared spectroscopic study of the phosphate mineral laueite. *Vibrational Spectroscopy*, **82**, 31–36.

Gagné O.C. and Hawthorne F.C. (2015) Comprehensive derivation of bond-valence parameters for ion pairs involving oxygen. *Acta Crystallographica*, **B71**, 562–578.

Golley P. and Williams R. (1995) *Cornish Mineral Reference Manual*. Endsleigh/Cornish Hillside Publications, UK.

Hoppe R. (1979) Effective coordination numbers (ECoN) and mean fictive ionic radii (MEFIR). *Zeitschrift für Kristallographie*, **150**, 23–52.

Kloprogge J.T and Wood B.J. (2020) *Handbook of Mineral Spectroscopy*. Elsevier, Amsterdam.

Mandarino J.A. (1981) The Gladstone-Dale relationship: Part IV. The compatibility concept and its application. *The Canadian Mineralogist*, **19**, 441–450.

Marzoni Fecia di Cossato Y., Orlandi P. and Pasero M. (1989) Manganese-bearing beraunite from Mangualde, Portugal: mineral data and structure refinement. *The Canadian Mineralogist*, **27**, 441–446.

Miyawaki R., Hatert F., Pasero M. and Mills S.J. (2021) Newsletter 63. *Mineralogical Magazine*, **85**, 910–915, http://doi.org/10.1180/mgm.2021.

Moore P.B. (1969) Basic ferric phosphates: A crystallochemical principle. *Science*, **164**, 1063–1064.

Moore P.B. (1970) Crystal chemistry of the basic iron phosphates. *American Mineralogist*, **55**, 135–169.

Moore P.B. and Kampf A.R. (1992) Beraunite: refinement, comparative crystal chemistry, and selected bond valences. *Zeitschrift für Kristallographie*, **201**, 263–281.

Moulder J.F., Stickle W.F., Sobol P.E. and Bomben K.D. (1995) *Handbook of X-ray Photoelectron Spectroscopy: A Reference Book of Standard Spectra for Identification and Interpretation of XPS Data*. Physical Electronics, Minnesota, USA, 261 pp.

Ondruš P. (1993) A computer program for analysis of X-ray powder diffraction patterns. *Materials Science Forum, EPDIC-2, Enschede*, **133–136**, 297–300.

Petříček V., Dušek M. and Palatinus L. (2020) *Crystallographic Computing System Jana2020*. Institute of Physics, CAS, Prague, Czech Republic.

Pouchou J. and Pichoir F. (1985) "PAP" (φρz) procedure for improved quantitative microanalysis. Pp. 104–106 in: *Microbeam Analysis* (J.T. Armstrong, editor). San Francisco Press, San Francisco.

Rhodes K. (2021) *Application Note: Analysis of Iron Oxidation States by XPS*. Accessed on March 14, 2021, at https://www.mccrone.com/mm/application-note-analysis-of-iron-oxidation-states-by-xps/.

Rigaku (2019) *CrysAlis CCD and CrysAlis RED*. Rigaku Oxford Diffraction Ltd, Yarnton, Oxfordshire, UK.

Scrivener R.C., Grant J.B., Hollick L.M. and Smith C.W. (2006) Nature and origin of the Great Perran Iron Lode, Perranporth area, Cornwall. *Geoscience in South-West England*, **11**, 255–256.

Sejkora J., Grey I.E., Kampf A.R., Price J.R. and Čejka J. (2016) Tvrdýite, $Fe^{2+}Fe_2^{3+}Al_3(PO_4)_4(OH_2)_4{\cdot}2H_2O$, a new phosphate mineral from Krásno near Horní Slavkov, Czech Republic. *Mineralogical Magazine*, **80**, 1077–1088.

Sheldrick G.M. (2015) SHELXT – Integrated space-group and crystal-structure determination. *Acta Crystallographica*, **A71**, 3–8.

Shirley D.A. (1972) High-resolution X-ray photoemission spectrum of the valence bands of gold. *Physical Review B*, **5**, 4709–4714.

Tvrdý J., Plášil J. and Škoda R. (2020) New crystal-chemical data on zincoberaunite from Krásno near Horní Slavkov (Czech Republic). *Journal of Geosciences*, **65**, 45–57.

Tvrdý, J., Plášil, J., Sejkora, J., Škoda, R., Vrtiška, L., Dolníček, Z., Petr, M. and Veselovský, F. (2021) Ferroberaunite, IMA 2021-036. CNMNC Newsletter 63. *Mineralogical Magazine*, **85**, 910–915, doi: https://doi.org/10.1180/mgm.2021.74.

Vrtiška L., Tvrdý J., Plášil J., Sejkora J., Škoda R., Chukanov N.V., Massanek A., Filip J., Dolníček Z. and Veselovský F. (2022) Redefinition of beraunite, $Fe_6^{3+}(PO_4)_4O(OH)_4{\cdot}6H_2O$, and discreditation of the name eleonorite: a re-investigation of type material from the Hrbek Mine (Czech Republic). *European Journal of Mineralogy*, **34**, 223–238.

Warr L.N. (2021) IMA–CNMNC approved mineral symbols. *Mineralogical Magazine*, **85**, 291–320.

Weiss S. (1989) Aktuelle Neufunde aus Cornwall. *Lapis*, **14**, 43–44.

Weiss S. (2019) Raritäten & Spezialitäten – von Bayldonit über Stokesit bis Woodwardit. *ExtraLapis*, **57**, 114–129.

https://doi.org/10.1180/mgm.2022.15 Published online by Cambridge University Press